RPE | Radiation Physics & Engineering
An International Peer-Reviewed Journal
Published by K.N. Toosi University of Technology
http://rpe.kntu.ac.ir
Research Article

Radiation Physics and Engineering 2021; 2(4):19–27
https://doi.org/10.22034/RPE.2021.312291.1044

Numerical simulation of supercritical water coolant flow in a GEN IV nuclear reactor by porous media approach

Danial Salehi[a], Gholamreza Jahanfarnia[a,*], Ehsan Zarifi[b]

[a] *Department of Nuclear Engineering, Science and Research Branch, Islamic Azad University, Tehran, Iran*
[b] *School of Reactor Safety, Nuclear Research and Science Institute, Tehran, Iran*

HIGHLIGHTS

- Numerical simulation of supercritical water coolant flow in a GEN IV nuclear reactor has been performed.
- Thermal-hydraulic analysis of a nuclear reactor has been done for safety purposes.
- Thermal hydraulic analysis of Canadian-SCWR has been conducted by numerically solving of conservation equations.
- There is a good agreement between our results and the reported results.

ABSTRACT

Canadian GEN IV Super Critical Water Reactor (Canadian-SCWR) is a combination version of conventional CANDU reactor with the using super critical water as coolant. Thermal-hydraulic analysis of a nuclear reactor is done to ensure that reactor will work in its safety margins. In this study, thermal hydraulic analysis of Canadian-SCWR is conducted by numerically solving of conservation equations by a porous media approach. The latest concept of Canadian-SCWR core was used for this purpose. In this concept, in each fuel bundles, super critical water flows in two pass and low pressure and low temperature heavy water moderator flows around fuel channel in the Calandria vessel, separately. Average axial temperature, density, heat capacity, pressure and velocity of supercritical water was estimated in two regions of fuel channels (two pass) i.e centeral flow tubes and the fuel rods channel. Compared to the literature, there is a good agreement between our results and the reported results.

KEYWORDS

Canadian-SCWR
Porous media approach
Tthermal-hydraulic analysis
Supercritical water coolant

HISTORY

Received: 27 October 2021
Revised: 2 December 2021
Accepted: 21 December 2021
Published: Autumn 2021

Nomenclature

A	Area (m^2)
g	Acceleration of gravity ($m.s^{-1}$)
k_e	Thermal Conductivity ($W.m^{-1}.°C$)
P	Pressure (Pa)
q	Heat (W)
q''	Heat flux ($W.m^{-2}$)
q'''	Volumetric Heat ($W.m^{-3}$)
R	Distributed resistant ($Pa.m^{-1}$)
t	Time (s)
T	Temperature (°C)
U	Internal energy ($J.kg^{-1}$)
ν	Velocity ($m.s^{-1}$)
V	Volume (m^3)
ρ	Density ($kg.m^{-3}$)
ϕ	Dissipation function ($W.m^{-3}$)
τ	Friction Tensor ($Pa.m.s^{-1}$)
γ	Porosity

Symbols and Operators

$\langle\ \rangle$	Volume averaging operator
$\{\ \}$	Surface averaging operator

Subscripts

A	Surface
f	Fluid
fs	Total fluid-solid interface
T	Total
V	Volumetric
x	Direction in Cartesian coordinate system
y	Direction in Cartesian coordinate system
z	Axial direction in Cartesian coordinate system

1 Introduction

Six reactor technologies, including supercritical water-cooled reactor (SCWR), have been selected under Generation IV Nuclear Energy System Development Project. The

*Corresponding author: rezajahan@yahoo.com

SCWRs are proposed in two different concept designs: i.e., pressure vessel supercritical water reactor (PV SCWR) and pressure tube supercritical water reactor (PT SCWR). Canada as a participant in Generation IV Nuclear Energy System program, has proposed pressure tube supercritical water reactor based on well-established CANDU reactors which defined as the Canadian-SCWR.

In Canadian SCWR, low pressure heavy water moderator is separated from super critical water coolant by a ceramic insulator which prevents heat loss from coolant to moderator and consequently drastic changes in moderator density (DoE, 2002; Yetisir et al., 2016).

Therefore, Canadian-SCWR has some benefits compared to pressure vessel SCWR (PV SCWR) which are explained as follows. Higher operating coolant temperature (e.g. 350 to 625 °C) in comparison to PV SCWR (e.g. 280 to 500 °C) makes this concept has a high thermal efficiency (about 48%). In addition, separation of coolant from the moderator makes high variation in supercritical water coolant has a low effect on the heavy water moderator and consequently is an advantage on the neutronic considerations.

Thermal-hydraulic analysis of Canadian SCWR has been conducted by various methods and codes such as single channel model, CATHENA and ASSERT-PV codes (Hummel and Novog, 2016; Ahmad et al., 2014; Domínguez et al., 2016; Wang and Wang, 2014; Peiman, 2017; Hummel, 2015). In recent years, porous media approach is taken into consideration as a powerful method to thermal-hydraulic analysis in complex geometries such as nuclear reactors. Based on this method, each fuel bundle is modeled into a network of lumped regions; each region is characterized by a volume average parameter. Therefore, complex geometries are easily defined and the thermal-hydraulic parameters and physical characteristics such as friction, shear stress, cross-flows, convective heat transfer and etc. can be accurately included in the simulations.

Recently, Jahanfarnia et al. have used this method to thermal-hydraulic analysis of various reactors such as VVER-1000, PV SCWR and HPLWR in different works (Rahimi et al., 2017; Rahimi and Jahanfarnia, 2014, 2016; Zarifi et al., 2013a,b; Tashakor et al., 2012, 2013).

In this work, the thermalhydraulic analysis of Canadian-SCWR core is investigated numerically by a porous media approach. This method is introduced to form the conservation equations by means of porosity concept within the control volume. The axial momentum equation is solved with high accuracy for single-phase coolant fluid. Despite of other methods, porous media approach calculates coolant temperature and not applied to calculate the fuel temperature profile (Rahimi and Jahanfarnia, 2016; Zarifi et al., 2013b).

2 Materials and Methods

2.1 Reactor core specifications

Geometry information of Canadian-SCWR concept is shown in Table 1. High efficiently re-entrant fuel channel specifications are collected in Table 2 (Hummel and Novog, 2016; Wu and Novog, 2015; Wu, 2014). Canadian SCWR core concept and fuel channel design are shown in Fig. 1. Reactor core consists of 336 fuel channels (Fig. 1), each fuel channel consists of a central flow tube, two concentric 32 numeric fuel rods rings around the central flow tube and two linear tubes that surrounded by a ceramic insulator and pressure tube. The supercritical water coolant flows through two direction in fuel channels. Firstly, the coolant flows downward through the central flow tube and then redirects in the bottom of the fuel channel, afterwards flows upward through the fuel rods (fuel rods channel), finally exits from the outlet plenum. Hence, thermalhydraulic analysis must be performed for two regions of fuel bundles, i.e. in central flow tube and fuel rods channel. As mentioned earlier, low pressure heavy water moderator flows around the fuel channels which its temperature and pressure is set to constant values.

Table 1: Reactor core specifications.

Parameter	Value
Moderator	Heavy water
Coolant	Light water
Inlet/Outlet temperature	350 °C/625 °C
Inlet/Outlet Pressure	25.7 MPa/25MPa
Thermal Power	2540 MW
Electric Power	1200 MW
Number of Channels	336
Fuel Assembly Length	5 m
Core Radius (with Reflector)	355 cm
Core Height (with Reflector)	650 cm
Flow direction in Center Flow Tube	Downwards
Flow direction among fuel rod	Upwards

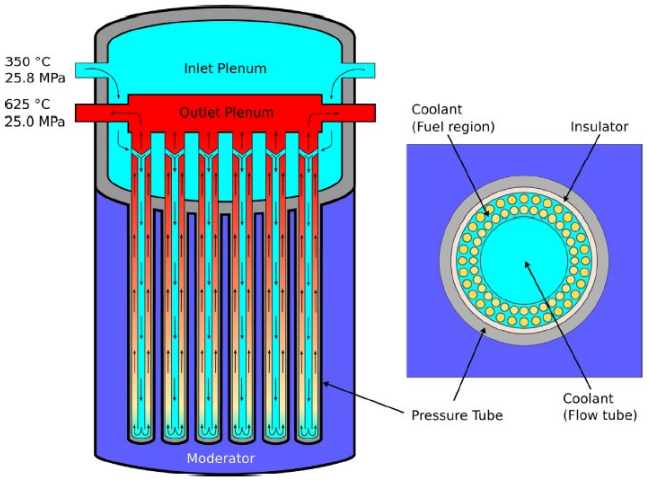

Figure 1: Canadian SCWR core concept and HERC Fuel Bundle Scheme (Hummel and Novog, 2016).

2.2 Porous media approach

In porous media approach, each fuel bundle is considered as a domain consisting of a single fluid and dispersed solid. These solids can generate or absorb heat. In an arbitrary point in this domain, a closed surface A_T can be associate

Table 2: Geometrical properties of fuel bundles.

Component	Dimension	Material
Center Tube coolant	4.60 cm radius	Light Water
Center Flow Tube	4.60 cm inner radius, 0.1 cm thick	Zr-modified 310 Stainless Steel
Inner Fuel pins (32)	0.415 cm radius, 5.4 cm pitch radius	15 wt% PuO_2 in ThO_2
Outer Fuel Pins (32)	0.440 cm radius, 6.575 cm pitch radius	12 wt% PuO_2 in ThO_2
Cladding	0.06cm thick	Zr-modified 310 Stainless Steel
Liner Tube	7.20cm radius; 0.05cm thick	Zr-modified 310 Stainless Steel
Insulator	7.25cm inner radius, 0.55cm thick	Yttria Stabilized Zirconia
Outer Liner	7.80cm inner radius; 0.05cm thick	Excel (Zirconium Alloy)
Pressure Tube	7.85 Cm inner radius; 1.2 cm thick	Excel (Zirconium Alloy)
Moderator	25 cm square lattice pitch	Heavy Water

with enclosing a volume V_T. The portion of V_T which contains the fluid is shown by V_T. A_{fs} is the total fluid-solid interface within the volume. A_f is the portion of A_T that fluid may flow through it. A schematic of the mentioned control volume is shown in Fig. 2.

Volume porosity γ_V is defined as the ratio of fluid volume V_f to the total volume V_T (solids and fluid). Therefore:

$$\gamma_V = \frac{V_f}{V_T} \tag{1}$$

Some formulations have introduced the additional concept of an area porosity or percentage area for flow associated with the surface enclosing the volume (Todreas and Kazimi, 2001). The surface porosity γ_A is defined by (Todreas Neil and Kazimi Mujid, 1990):

$$\gamma_A = \frac{A_f}{A_T} \tag{2}$$

where the portion of A_T which is occupied by the fluid is A_f. Differential forms of mass, linear momentum and energy (in terms of internal energy), conservation equations in a flow field are introduced as follows (Rahimi and Jahanfarnia, 2016; Todreas and Kazimi, 2001; Todreas Neil and Kazimi Mujid, 1990):

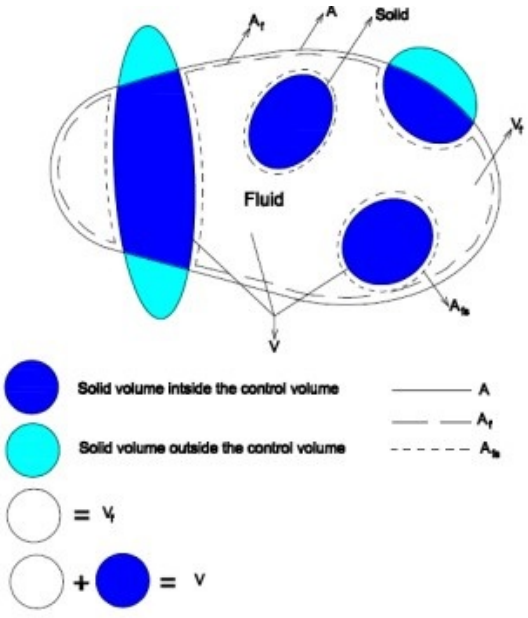

Figure 2: A domain consisting of a single-phase fluid with stationary solids (Rahimi and Jahanfarnia, 2016).

$$\frac{\partial \rho}{\partial t} + \nabla.(\rho \vec{v}) = 0 \tag{3}$$

$$\frac{\partial (\rho \vec{v})}{\partial t} + \nabla.(\rho \vec{v}\vec{v}) = -\nabla P + \nabla.\bar{\bar{\tau}} + \rho \vec{g} \tag{4}$$

$$\frac{\partial (\rho U)}{\partial t} + \nabla.(\rho U \vec{v}) = -\nabla.\vec{q''} + q''' - P\nabla.\vec{v} \tag{5}$$

By definition of porosity and performing the volume and surface averaging, the conservation equation of mass and momentum (Eqs. (3) and (4)) can be rewritten as:

$$\gamma_V \frac{\partial^i \langle \rho \rangle}{\partial t} + \frac{1}{V_T}\int_{A_f} \rho \vec{v}.\vec{n}\, \mathrm{d}A = 0 \tag{6}$$

$$\begin{aligned} &\gamma_V \frac{\partial\, ^i\langle \rho \vec{v} \rangle}{\partial t} + \frac{1}{V_T}\int_{A_f} \rho \vec{v}(\vec{v}.\vec{n})\, \mathrm{d}A \\ &= \gamma_V\, ^i\langle \rho \rangle \vec{g} + \frac{1}{V_T}\int_{A_f} (-P.\vec{n} + \bar{\bar{\tau}}.\vec{n})\, \mathrm{d}A + \gamma_V\, ^i\langle \vec{R} \rangle \end{aligned} \tag{7}$$

The resistance force exerted on the fluid by the dispersed solid per unit volume of fluid is defined as the distributed resistance $\vec{R}$ and shown by:

$$\int_{V_f} \vec{R}\, \mathrm{d}V = \int_{A_f} (-P.\vec{n} + \bar{\bar{\tau}}.\vec{n})\, \mathrm{d}A \tag{8}$$

An equivalent but in the opposite direction force is applied on the dispersed solid by the fluid that is defined as effective drag force per unit volume of fluid. For axial flow, if there is no form drag and by applying a force balance, it can be obtained:

$$\begin{aligned} ^i\langle R_z \rangle &= \frac{1}{V_f}\vec{k}.\int_{A_{fs}} \bar{\bar{\tau}}.\vec{n}\, \mathrm{d}A \\ &= -\frac{\Delta P_{friction} A_f}{V_f} = -\frac{\Delta P_{friction}}{\Delta z} \\ &= f\frac{\Delta z}{D_e}\frac{^i\langle \rho \rangle\, ^i\langle v_z \rangle^2}{2} \end{aligned} \tag{9}$$

where symbols $\langle\ \rangle$ and $^i\langle\ \rangle$ indicate that the average is associated with the whole volume and the fluid flow volume, respectively, while the mathematical symbol $\{\ \}$ indicates that the average is associated with the surface. By applying the theorem of local volume averaging of a divergence to $-\bigtriangledown.\vec{q''}$ in Eq. (5) and then expressing the divergence of

an intrinsic local volume average, the following equation is obtained:

$$-\langle\nabla.\vec{q''}\rangle = -\nabla.\langle\vec{q''}\rangle - \frac{1}{V_T}\int_{A_{fs}} \vec{q''}.\vec{n}\,\mathrm{d}A = -\frac{1}{V_T}\int_{A_f} \vec{q''}.\vec{n}\,\mathrm{d}A - \frac{1}{V_T}\int_{A_{fs}} \vec{q''}.\vec{n}\,\mathrm{d}A \tag{10}$$

The first surface integral in Eq. (10) represents the conduction heat transfer across the fluid surface, A_f , and the second represents the conduction heat transfer across all fluid-solid interfaces, A_{fs}, By using Fourier's conduction law ($\int_{A_f} k_e\vec{n}.\nabla T\,\mathrm{d}A = -\int_{A_f} \vec{q''}.\vec{n}\,\mathrm{d}A$), we will have:

$$-\langle\nabla.\vec{q''}\rangle = \frac{1}{V_T}\int_{A_f} k_e\vec{n}.\nabla T\,\mathrm{d}A - \frac{1}{V_T}\int_{A_{fs}} \vec{q''}.\vec{n}\,\mathrm{d}A \tag{11}$$

Equivalent dispersed heat source (or sink) per unit volume of the fluid, q'''_{rb}, can be defined as $\int_{V_f} q'''_{rb}\,\mathrm{d}V = \int_{A_{fs}} \vec{q''}.\vec{n}\,\mathrm{d}A$. By a procedure analogous and by using the linear momentum equation, and using the definition of q'''_{rb}, we will have:

$$\gamma_V\frac{\partial\,{}^i\langle\rho U\rangle}{\partial t} + \frac{1}{V_T}\int_{A_f}\rho U\vec{v}.\vec{n}\,\mathrm{d}A = -\gamma_V\langle P\nabla.\vec{v}\vec{g}\rangle + \frac{1}{V_T}\int_{A_f} k_e\vec{n}.\nabla T\,\mathrm{d}A + \gamma_V\Big({}^i\langle q''_{rb}\rangle + {}^i\langle q'\rangle + {}^i\langle\phi\rangle\Big) \tag{12}$$

The integral form of conservation equation is simplified by taking $V_T = \Delta x\Delta y\Delta z$ and porosity definition in Cartesian coordinate system and performing the volume and surface averaging as bellow (Rahimi et al., 2017; Rahimi and Jahanfarnia, 2016):

$$\underbrace{\gamma_V\frac{\partial\,{}^i\langle\rho\rangle}{\partial t}}_{\text{Rate of mass increase}} + \underbrace{\frac{\Delta_x\big(\gamma_{Ax}\{\rho v_x\}\big)}{\Delta x}}_{\text{Net outflux in x direction}} + \underbrace{\frac{\Delta_y\big(\gamma_{Ay}\{\rho v_y\}\big)}{\Delta y}}_{\text{Net outflux in y direction}} + \underbrace{\frac{\Delta_z\big(\gamma_{Az}\{\rho v_z\}\big)}{\Delta z}}_{\text{Net outflux in z direction}} = 0 \tag{13}$$

$$\begin{aligned}\gamma_V\frac{\partial\,{}^i\langle\rho v_z\rangle}{\partial t} &+ \frac{\Delta_x\big(\gamma_{Ax}{}^{i(x)}\{\rho v_z v_x\}\big)}{\Delta x} + \frac{\Delta_y\big(\gamma_{Ay}{}^{i(y)}\{\rho v_z v_y\}\big)}{\Delta y} + \frac{\Delta_z\big(\gamma_{Az}{}^{i(z)}\{\rho v_z v_z\}\big)}{\Delta z}\\ &= -\gamma_V{}^i\langle\rho\rangle g_z - \frac{\Delta_z\big(\gamma_{Az}{}^{i(z)}\{P\}\big)}{\Delta z} + \frac{\Delta_x\big(\gamma_{Ax}{}^{i(x)}\{\tau_{xz}\}\big)}{\Delta x} + \frac{\Delta_y\big(\gamma_{Ay}{}^{i(y)}\{\tau_{yz}\}\big)}{\Delta y}\\ &+ \frac{\Delta_z\big(\gamma_{Az}{}^{i(z)}\{\tau_{zz}\}\big)}{\Delta z} + \gamma_V{}^i\langle R_z\rangle\end{aligned} \tag{14}$$

where $\gamma_V\dfrac{\partial\,{}^i\langle\rho v_z\rangle}{\partial t}$ shows the rate of increase of linear momentum of the fluid mass in V_T, and the other three terms in the left side of the equation show the net linear momentum outflux through the surface enclosing V_T. In the right side of the equation, $\gamma_V{}^i\langle\rho\rangle g_z$ stands for the body force due to gravity acting on the fluid mass, the second term shows the surface force due to normal fluid stress (presure) acting on the fluid mass, and the next three terms are the surface force due to the fluid shear stress acting on the fluid mass. Also, the last term ,$\gamma_V{}^i\langle R_z\rangle$, shows the surface force exerted on the fluid by the dispersed solid.

$$\begin{aligned}\gamma_V\frac{\partial\,{}^i\langle\rho U\rangle}{\partial t} &+ \frac{\Delta_x\big(\gamma_{Ax}{}^{i(x)}\{\rho U v_x\}\big)}{\Delta x} + \frac{\Delta_y\big(\gamma_{Ay}{}^{i(y)}\{\rho U v_y\}\big)}{\Delta y} + \frac{\Delta_z\big(\gamma_{Az}{}^{i(z)}\{\rho U v_z\}\big)}{\Delta z}\\ &= -\gamma_V{}^i\Big\langle\rho\Big(\frac{\partial v-x}{\partial x} + \frac{\partial v-y}{\partial y} + \frac{\partial v-z}{\partial z}\Big)\Big\rangle + \frac{\Delta_x\big(\gamma_{Ax}{}^{i(x)}\{k_e\frac{\partial T}{\partial x}\}\big)}{\Delta x} + \frac{\Delta_y\big(\gamma_{Ay}{}^{i(y)}\{k_e\frac{\partial T}{\partial y}\}\big)}{\Delta y}\\ &+ \frac{\Delta_z\big(\gamma_{Az}{}^{i(z)}\{k_e\frac{\partial T}{\partial z}\}\big)}{\Delta z} + \gamma_V\big({}^i\langle q'''_{rb}\rangle + {}^i\langle q'''\rangle + {}^i\langle\phi\rangle\big)\end{aligned} \tag{15}$$

where $\gamma_V\dfrac{\partial\,{}^i\langle\rho U\rangle}{\partial t}$ is rate of increase of internal energy of the fluid mass in V_T, and the next three terms of the left side are net internal energy outflux through the surface enclosing V_T. Moreover, in the right side of the equation, the first term shows the reversible rate of pressure work when the density is not constant, the next three terms are heat conduction through the portion of the surface that is free to fluid flow, and the last term is the sum of the heat liberated (or observed) due to emmersed solid, extraneous internal sources and viscous dissipative effects. Also:

$$\begin{aligned}\Delta_x &= (\,)_{x+\frac{\Delta_x}{2}} - (\,)_{x-\frac{\Delta_x}{2}}\\ \Delta_y &= (\,)_{y+\frac{\Delta_y}{2}} - (\,)_{y-\frac{\Delta_y}{2}}\\ \Delta_z &= (\,)_{z+\frac{\Delta_z}{2}} - (\,)_{z-\frac{\Delta_z}{2}}\end{aligned} \tag{16}$$

In porous media approach, thermalhydraulic parameters are achieved for each fuel bundle in the core, finally average results are calculated for whole reactor core. Appropriate boundary conditions such as inlet temperature, density and velocity and outlet pressure are required for thermalhydraulic analysis (see Table 3).

Another requirement for thermal-hydraulic analysis is power distribution across the reactor core, including radial and axial distribution. We considered channel power distribution and average axial fuel bundles power of the Canadian-SCWR reported by Hummel et al (Hummel and Novog, 2016), that fuel bundles number in the core is shown in Fig. 3 and we used the same. The thermophysical properties of supercritical water are main challenge in thermal-hydraulic analysis of this reactor especially in pseudo-critical region of water. The thermophysical properties, such as density, heat capacity, thermal conductivity and etc. change rapidly with increasing temperature. So in each axial section, the thermodynamic properties must be obtained with temperature variation.

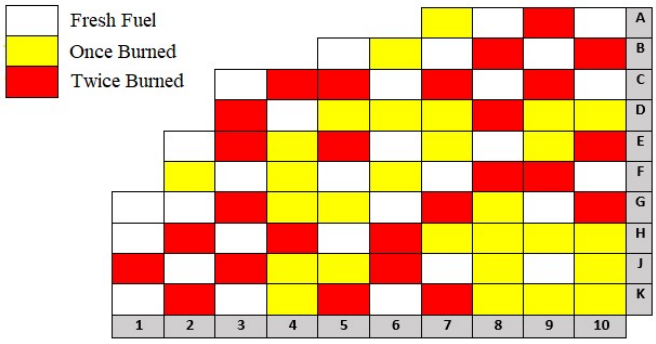

Figure 3: Canadian SCWR quarter core model (without reflector) with defined number for each fuel-bundle (Ahmad et al., 2014).

Table 3: Selected boundary conditions for calculation.

Properties	Value
Inlet temperature	350 (°C)
Outlet Pressure	25 (MPa)
Inlet axial-velocity	1.56 (m/s)

In this work the numerical solution of conservation equations of mass, momentum and energy (Eqs. (13) to (15)) were performed by Finite Volume Method in 100 axial mesh (control volume) across fuel bundles. The flow chart of steady state thermo-hydraulic analysis in the reactor core is shown in Fig. 4. By implementing a combination of conservation equations for the entire lattice nodalization, a three-diagonal matrix is formed, which is solved despite the initial and boundary conditions based on the mentioned algorithm by Gauss-Jordan way. First, the pressure is calculated by using continuity equation in each nod and then axial velocity in all nodes is calculated by having the pressure of each point. Finally, the temperature are extracted using the energy equation. The remaining thermal-hydraulic variables are calculated using IAPWS-IF97.

According to this algorithm, a computer code was developed in C# language and thermo-hydraulic parameters of supercritical water coolant were calculated in this reactor. More details about conservation equations and porous media approach present in pervious works (Todreas and Kazimi, 2001; Zarifi et al., 2013b; Rahimi and Jahanfarnia, 2014, 2016; Rahimi et al., 2017; Salehi et al., 2020).

2.3 Average clad wall and fuel temperature calculation in the reactor core

Since the porous media method is not applied to calculate the fuel temperature gradients, so for fuel and clad temperature calculation, heat transfer equation for fuel and clad was discretized by Finite volume method and solved numerically. By using the fuel rod heat conduction model, implies a fuel heating model and a heat transfer model from a heated wall to the coolant, the temperature distribution in the fuel rod is calculated at each axial level. Given that axial heat conduction is negligible compared to the radial direction. So the heat balance equation is approximated with a first order finite-difference equation (Zarifi et al., 2013a; Salehi et al., 2020). So fuel and clad temperature distribution are obtained by:

$$\frac{1}{r}\frac{\mathrm{d}}{\mathrm{d}r}\left(Kr\frac{\mathrm{d}T}{\mathrm{d}r}\right) = -q''' \tag{17}$$

where K is thermal conductivity coefficient that for fuel temperature calculation is replaced by K_f and for clad temperature distribution is replaced by K_c and $q''' = 0$. Fuel and clad thermal conductivity coefficient calculated as a function of temperature thats exists in literature (Salaun, 2018; Peiman, 2017).

2.4 Heat transfer correlation

Due to dependence of heat transfer coefficient to thermophysical properties of coolant such heat capacity, density, dynamic viscosity and thermal conductivity, and this properties rapidly change near pseudo-critical region, estimation of heat transfer is a main challenge in Canadian SCWR.

Since bishop correlation was achieved within the condition similar to Canadian SCWR concept, so Bishop Correlation was used to obtain heat transfer coefficient. This correlation is as follow (Liu et al., 2013; Peiman, 2017; Salehi et al., 2020):

$$\begin{aligned} Nu_B &= \frac{hD_h}{k} \\ &= 0.0069\,\mathrm{Re}_B^{0.9}.\mathrm{Pr}_B^{0.66}\left(\frac{\rho_{wal}}{\rho_B}\right)\left(\frac{z+2.4D_h}{z}\right) \end{aligned} \tag{18}$$

3 Results and Discussion

One dimensional averaged thermalhydraulic results (in average core) obtained from porous media approach are presented as follows. Change of coolant density in compare with the literature is shown in the Fig. 5. This figure shows that by increasing coolant temperature, the volume of coolant is increased and consequently density will be decreased. The coolant density is decreased to 538 $\mathrm{kg.m^{-3}}$ in the bottom of fuel channels (at the end of centre flow tube) and reaches to 69 $\mathrm{kg.m^{-3}}$ in top of the fuel channels, as this drastic reduction in density is a main feature of the Canadian-SCWR.

Change of coolant velocity during passing through the fuel channel is shown in the Fig. 6. As can be observed, coolant velocity in the central flow tube will be increased too slightly (about 0.5 $\mathrm{m.s^{-1}}$) and among fuel rods (fuel rods channel) increases, according to the continuity equation, to 10 $\mathrm{m.s^{-1}}$, due to rapid changes of fluid density in fuel rods region. At the end of the fuel channel, the coolant velocity in the centre flow tube is different from the fuel rods region due to changes in cross-sectional area.

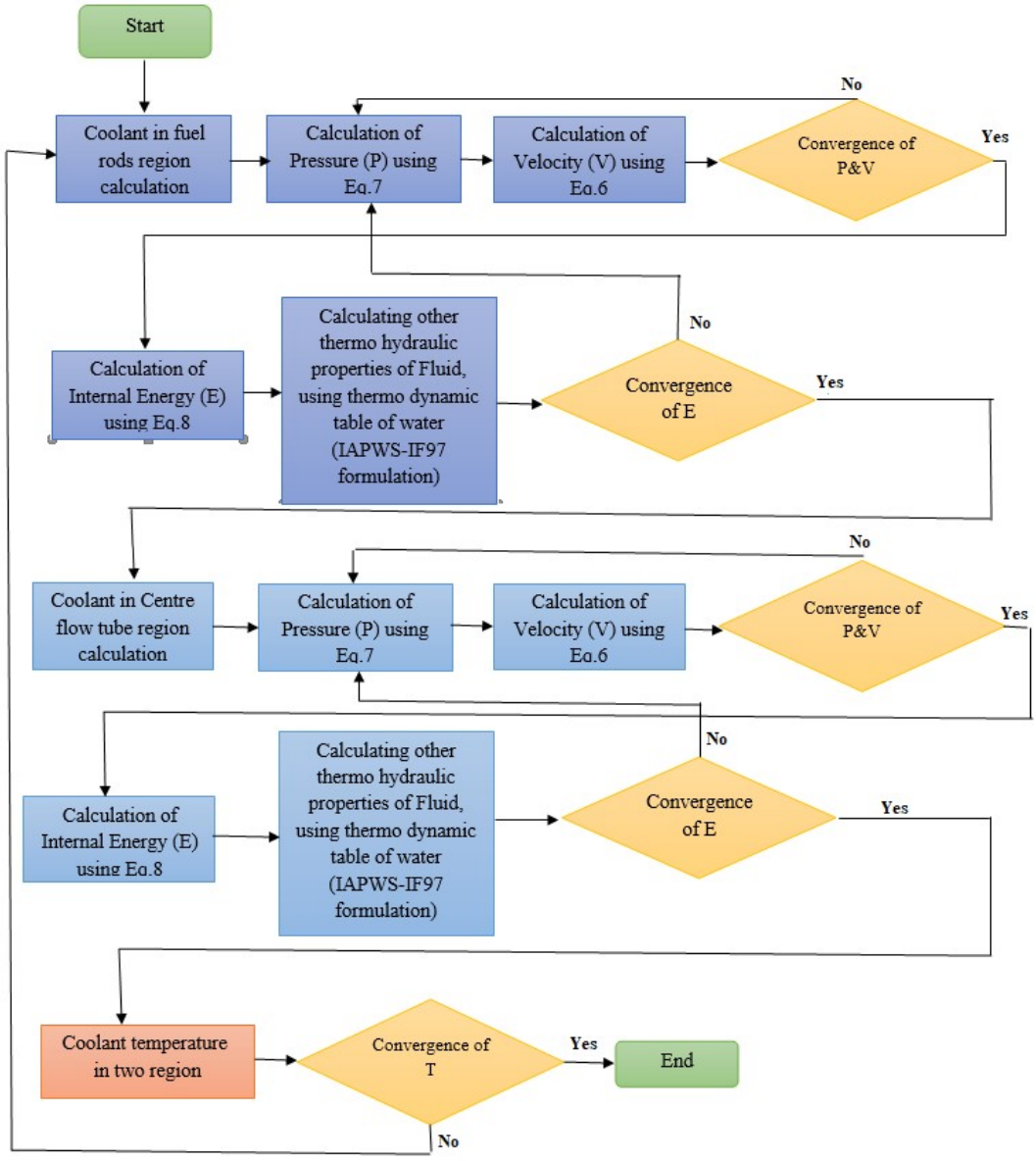

Figure 4: Flowchart of the calculation procedure.

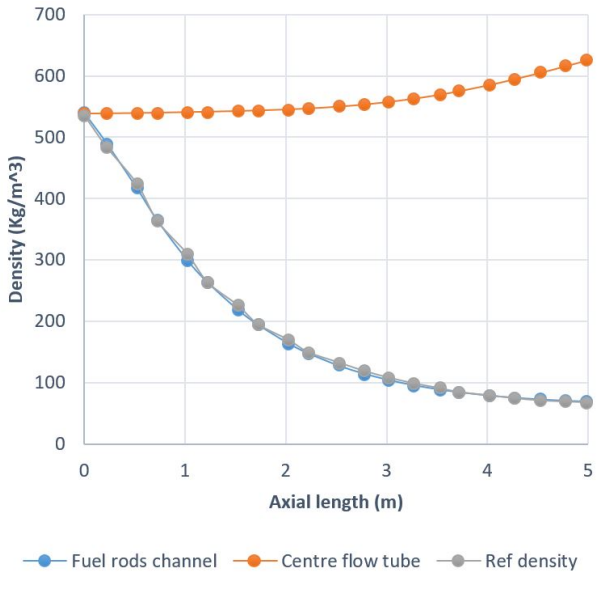

Figure 5: Average coolant density in the core.

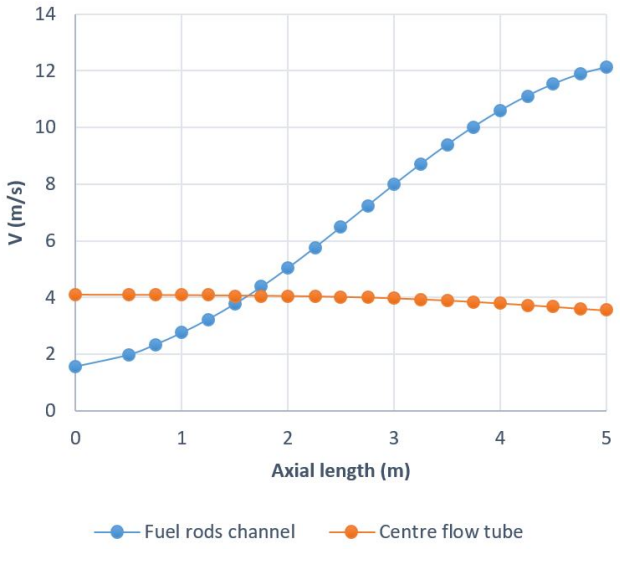

Figure 6: Average coolant velocity in the core.

Pressure drop of the coolant during passing through the fuel channels is due to friction between water and fuel rods walls, the body force, accelerator and etc. .The average pressure variation of coolant in the core is shown in the Fig. 7. As can be seen, the coolant pressure drop in the central flow tube is lower than fuel rods channel. The total reduction in coolant pressure across the fuel channel is about 0.7 MPa.

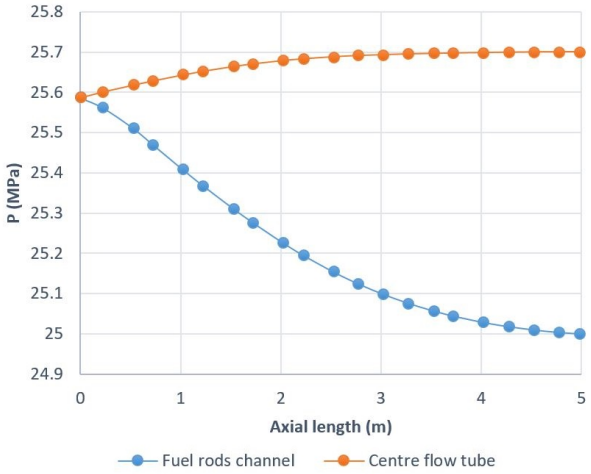

Figure 7: Average coolant pressure in the core.

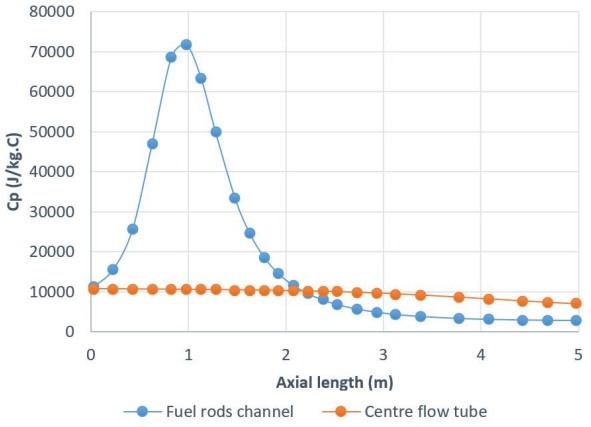

Figure 8: Average specific heat capacity of the coolant in the core.

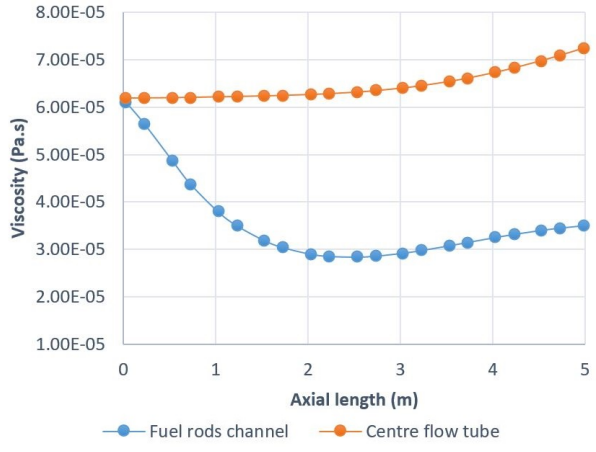

Figure 9: Axial variation of viscosity in the core.

The specific heat capacity variation of coolant is shown in the Fig. 8. According to this figure, it can be seen that the heat capacity changes is very small in the central flow tube. In fuel rods channel, heat capacity changes strongly with coolant temperature increment in axial direction, especially in pseudo-critical region of water. In this region, the results show a peak in the specific heat capacity values due to reaching water to pseudo-critical point in 0.725 m (i.e., where the temperature is 384 °C).

The axial variations of coolant viscosity is shown in the Fig. 9. As can be seen, the viscosity decreases with increasing temperature, especially in the fuel rods channel due to higher temperature variation in this region.

To fuel centreline temperature calculation, fuel rod heat conduction equation was solved in 10 radial nods, axial distribution of fuel temperature in different radial nodes is presented in Fig. 10.

Fig. 11-a is shown the axial variation of coolant temperature in the central flow tube and temperature values in the fuel rods channel are compared with the literature (Hummel and Novog, 2016; Hummel, 2015; Wu, 2014). As can be observed the coolant with temperature of 350 °C enters the centre flow tube (from the top), then enters the fuel rods channel with temperature of 370 °C. Then, the coolant flows upward and leaves the fuel rods channel with average temperature of 613 °C. The relative differences in coolant temperature between the porous media approach and the results of the literature is shown in Fig. 11-b. There is little difference between the obtained results and the data reported in the literature, which is due to the type of analysis.

Figures 12-a and 12-b show the calculated average coolant density, clad wall temperature and fuel centreline temperature compared with the data reported in the literature (Hummel, 2015). As it can be seen the comparison shows good agreement.

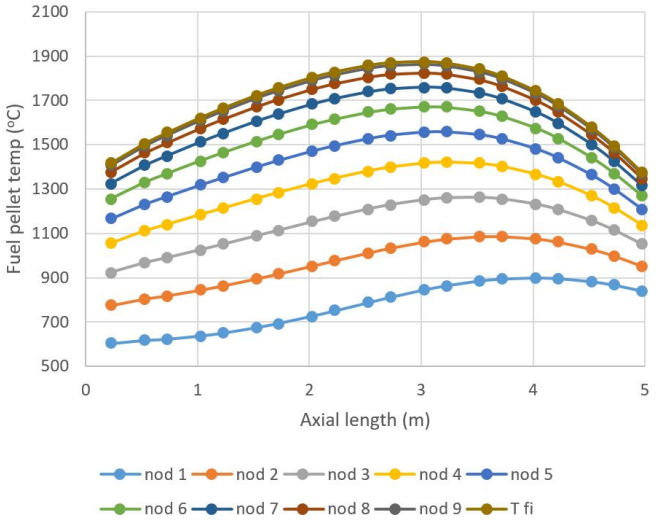

Figure 10: Axial distribution of fuel temperature in different radial nodes.

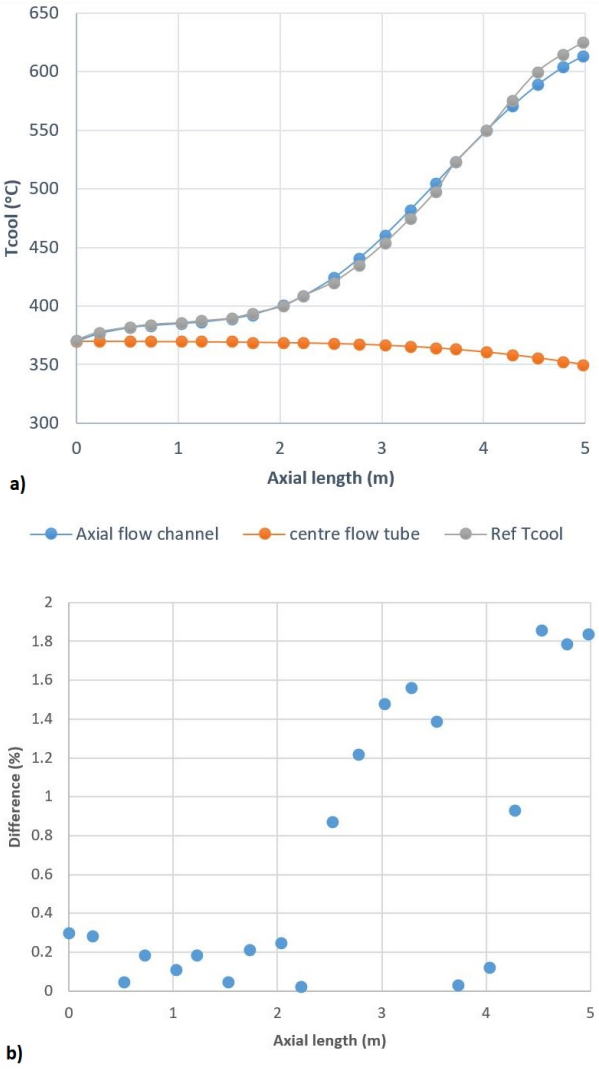

Figure 11: a) Comparison of average coolant temperature changes in the core with literature. b) Difference (%) between coolant temperature calculation by porous media approach and the data of the literature in fuel rods channel.

4 Conclusion

Thermal-hydraulic Analysis of the Canadian-SCWR was performed by porous media approach. Newest proposed fuel channel design (HERC) was used for this analysis which the main feature of HERC is presence of two path for coolant. Therefore, conservation equations of the mass, momentum and energy were solved in two regions of the fuel channel by a coupling procedure. As a result, coolant temperature, pressure and density change were calculated in central flow tube and fuel rods channel by porous media approach, in Steady state condition for the first time.

Our results show that coolant temperature reaches to pseudo critical point in 0.725 m length of the core, therefore rapid changes in thermo-physical properties of the coolant (such as density and specific heat capacity) are can be seen in this region. The average output coolant temperature andthe average increasing of coolant temperature in center flow tube were estimated to 613 °C and 20 °C respectively. Average coolant pressure drops (Pin-Pout) was calculated to 0.7 MPa in the core. Comparing our results with literature shows a good agreement.

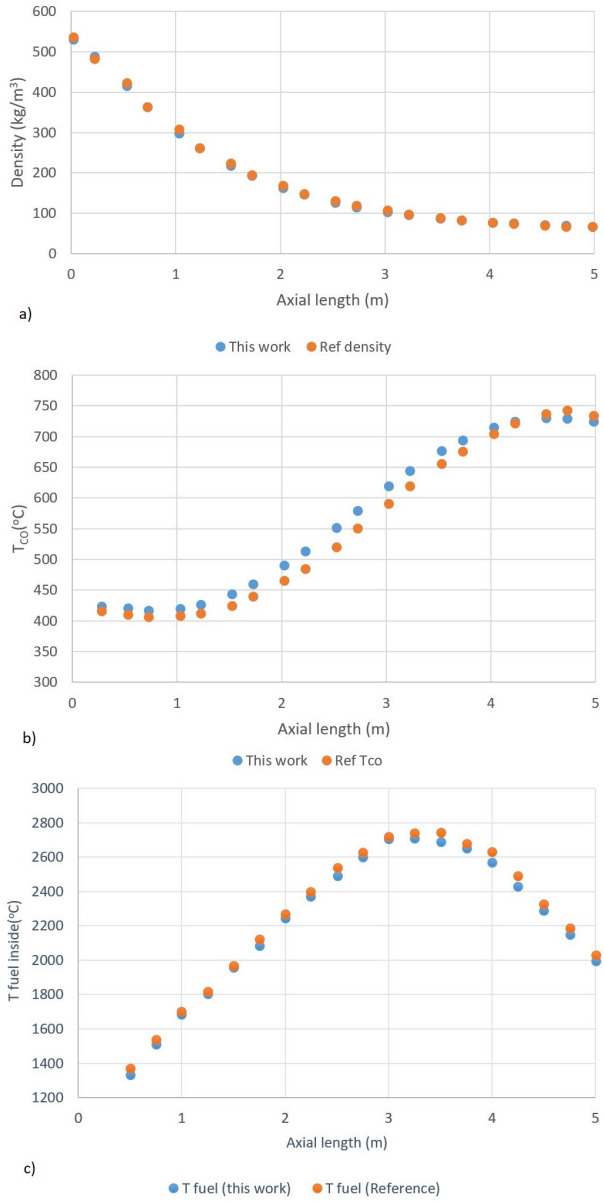

Figure 12: a) Average coolant density in the core obtained by porous media approach compared to data reported in the literature. c, d) Average clad wall temperature and fuel centreline temperature compared with data reported in the references.

References

Ahmad, A., Cao, L., and Wu, H. (2014). Coupled analysis and improvements for Canadian-SCWR core design. *Nuclear Engineering and Design*, 268:104–112.

DoE, U. (2002). A technology roadmap for generation IV nuclear energy systems. *http://gif.inel.gov/roadmap/pdfs/gen_iv_roadmap.pdf*.

Domínguez, A. N., Onder, N., Rao, Y., et al. (2016). Evolution of the Canadian SCWR fuel-assembly concept and assessment of the 64 element assembly for thermalhydraulic performance. *CNL Nuclear Review*, 5(2):221–238.

Hummel, D. W. (2015). Transient neutronic-thermalhydraulic coupling in a PT-SCWR. *Hamilton, Ontario, Canada*.

Hummel, D. W. and Novog, D. R. (2016). Coupled 3d neutron kinetics and thermalhydraulic characteristics of the Canadian supercritical water reactor. *Nuclear Engineering and Design*, 298:78–89.

Liu, X., Yang, T., and Cheng, X. (2013). Thermal-hydraulic analysis of flow blockage in a supercritical water-cooled fuel bundle with sub-channel code. *Annals of Nuclear Energy*, 59:194–203.

Peiman, W. (2017). *Study on specifics of thermalhydraulics and neutronics of pressure-channel supercritical water-cooled reactors (SCWRs)*. PhD thesis.

Rahimi, M. and Jahanfarnia, G. (2014). Thermal-hydraulic core analysis of the VVER-1000 reactor using a porous media approach. *Journal of Fluids and Structures*, 51:85–96.

Rahimi, M. and Jahanfarnia, G. (2016). Thermo-hydraulic analysis of the supercritical water-cooled reactor core by porous media approach. *The Journal of Supercritical Fluids*, 110:275–282.

Rahimi, M., Jahanfarnia, G., and Vosoughi, N. (2017). Thermal–hydraulic analysis of nanofluids as the coolant in supercritical water reactors. *The Journal of Supercritical Fluids*, 128:47–56.

Salaun, F. (2018). *Assessment and optimization of the Canadian SCWR reactivity control systems through reactor physics and thermal-hydraulics coupling*. PhD thesis.

Salehi, D., Jahanfarnia, G., and Zarifi, E. (2020). Thermal-hydraulic analysis of Al_2O_3 nanofluid as a coolant in Canadian supercritical water reactor by porous media approach. *Nuclear Engineering and Design*, 368:110825.

Tashakor, S., Salehi, A., Jahanfarnia, G., et al. (2012). Neutronic analysis of HPLWR fuel assembly cluster. *Annals of Nuclear Energy*, 50:38–43.

Tashakor, S., Salehi, A., Jahanfarnia, G., et al. (2013). Thermal–hydraulic analysis of HPLWR fuel assembly cluster. *The Journal of Supercritical Fluids*, 77:91–99.

Todreas, N. E. and Kazimi, M. S. (2001). *Nuclear systems: elements of thermal hydraulic design*. Taylor & Francis.

Todreas Neil, E. and Kazimi Mujid, S. (1990). Nuclear Systems I: Thermal Hydraulic Fundamentals.

Wang, D. and Wang, S. (2014). A preliminary CATHENA thermalhydraulic model of the Canadian SCWR for safety analysis. *AECL Nuclear Review*, 3(01):9–16.

Wu, Y. (2014). *Prediction of the response of the Canadian Super Critical Water reactor to potential Loss of Forced Flow Scenarios*. PhD thesis.

Wu, Y. and Novog (2015). *Prediction of response of the Canadian super critical water reactor to potential loss of forced flow scenarios, 7^{th} International Symposium on Supercritical Water-Cooled Reactors (ISSCWR-7), Helsinki, Finland*. PhD thesis.

Yetisir, M., Gaudet, M., Pencer, J., et al. (2016). Canadian supercritical water-cooled reactor core concept and safety features. *CNL Nuclear Review*, 5(2):189–202.

Zarifi, E., Jahanfarnia, G., and Veysi, F. (2013a). Subchannel analysis of nanofluids application to VVER-1000 reactor. *Chemical Engineering Research and Design*, 91(4):625–632.

Zarifi, E., Jahanfarnia, G., and Veysi, F. (2013b). Thermal–hydraulic modeling of nanofluids as the coolant in VVER-1000 reactor core by the porous media approach. *Annals of Nuclear Energy*, 51:203–212.